SUPPORTING INFORMATION

Batteries for Efficient Energy Extraction from a Water Salinity Difference

Fabio La Mantia[a†], *Mauro Pasta*[a,b†], *Heather D. Deshazer*[a], *Bruce E. Logan*[c] *and Yi Cui*[a*]

[a] Department of Materials Science and Engineering, Stanford University, Stanford, CA 94305, USA

[b] Dipartimento di Chimica Inorganica, Metallorganica e Analitica "Lamberto Malatesta", Università degli Studi di Milano, Via Venezian 21, 20133 Milan, Italy

[c] Department of Civil and Environmental Engineering, Penn State University, University Park, PA 16802, USA

[†] These authors contributed equally to this work.

[*] Correspondence and requests for materials should be addressed to Y.C. (yicui@stanford.edu)

1. Electrochemical Thermodynamics details

In Figure S1a is reported the schematic representation of the electrochemical system AgCl / $Na_2Mn_5O_{10}$. The two separate electrochemical reactions can be written as:

$$\begin{aligned} 5MnO_{2(\alpha)} + 2Na^{+}{}_{(\varepsilon)} + 2e^{-}{}_{(\alpha)} &\rightleftarrows Na_2Mn_5O_{10(\alpha)} \\ 2AgCl_{(\beta')} + 2e^{-}{}_{(\alpha')} &\rightleftarrows 2Ag_{(\alpha')} + 2Cl^{-}{}_{(\varepsilon)} \end{aligned} \qquad \text{(S1)}$$

where α is the $Na_{2-x}Mn_5O_{10}$ phase, ε the electrolyte phase, β' the AgCl phase, and α' the Ag phase. The potential of the two reactions with respect to the normal hydrogen electrode (NHE) is given by:

$$\begin{aligned} E_{+} &= E_{+,0} + \frac{RT}{F}\ln\left[\frac{a_{Na,\varepsilon}}{a_{Na,\alpha}}\right] \\ E_{-} &= E_{-,0} - \frac{RT}{F}\ln\left[a_{Cl,\varepsilon}\right] \end{aligned} \qquad \text{(S2)}$$

where E_+ and E_- are the potentials of the electrodes, $E_{+,0}$ and $E_{-,0}$ the standard potentials of the electrodes, $a_{Na,\alpha}$ the activity of the sodium in the solid phase α, $a_{Na,\varepsilon}$ the activity of the sodium ions in the electrolyte, $a_{Cl,\varepsilon}$ the activity of the chlorides in the electrolyte. The difference between the two potentials is ΔE. If the activity of sodium in the solid phase is fixed (no current flowing), one obtains:

$$\Delta E = \Delta E_0\left(a_{Na,\alpha}\right) + 2\frac{RT}{F}\ln\left[c_{NaCl}\right] + 2\frac{RT}{F}\ln\left[\gamma_{NaCl}\right] \qquad \text{(S2)}$$

where ΔE_0 is the standard cell voltage, c_{NaCl} the concentration of NaCl, γ_{NaCl} the mean activity coefficient of NaCl. Equation S2 can be rearranged as:

$$\Delta E^{*} = \Delta E - 2\frac{RT}{F}\ln\left[c_{NaCl}\right] = \Delta E_0 + 2\frac{RT}{F}\ln\left[\gamma_{NaCl}\right] \qquad \text{(S3)}$$

where the variable ΔE^{*} is defined for convenience in graphing. ΔE^{*} can be calculated once the value of ΔE is measured at the various concentrations. In general, ΔE^{*} can be used to obtain the value of ΔE_0 and

the dependence of γ_{NaCl} on c_{NaCl}, using the Debye-Hückel law. For diluted solutions of completely dissociated salts, the mean activity coefficient of the salt follows the Debye-Huckel law:

$$\ln[\gamma_{NaCl}] = -\frac{A\sqrt{c_{NaCl}}}{1 + B\sqrt{c_{NaCl}}} \qquad \text{(S4)}$$

From the fitting of the experimental data reported in Figure S2a, the value of $\Delta E_0 \approx 0.4127$ V is obtained. In equation S4, the value of A is equal to 36.59 $cm^{1.5}$ $mol^{-0.5}$, in good agreement with the theoretical prediction of 37.65 $cm^{1.5}$ $mol^{-0.5}$. B is proportional to the mean hydrodynamic radius of the ions. The value of B obtained is 12.27 $cm^{1.5}$ $mol^{-0.5}$, which corresponds to a hydrodynamic radius equal to 1.2 Å. Equations S3 and S4 were fitted to the data in the concentration range between 1 and 20 mM. The potential difference at lower concentrations is strongly affected by impurities, such as oxygen, while at high concentrations equation S4 is outside the range of validity, as the Debye-Huckel law is only valid for diluted solutions. Using the value we obtained for ΔE_0, in Figure S2b, the value of γ_{NaCl} at different concentration is reported. The mean activity coefficient can be used to calculate the mixing energy of two solutions at different volumetric fractions. The Gibbs free energy of mixing is equal to:

$$\frac{\Delta G}{2RT} = \frac{\Delta G_{id}}{2RT} + \ln\left[\frac{\gamma_T}{\gamma_C^x \gamma_D^{1-x}}\right] \qquad \text{(S5)}$$

where ΔG_{id} is the one reported in equation (2) of the main text, γ_T the mean activity coefficient of NaCl in the mixed solution, γ_C the mean activity coefficient of NaCl in the concentrated solution (sea water), and γ_D the mean activity coefficient of NaCl in the diluted solution (river water). The error committed by using equation (1) as an estimate, instead of equation (S5), is at most 22 J dm^{-3}, which corresponds to about 2% of the total Gibbs energy.

It is possible to repeat the same calculation for the system $LiFePO_4$ / AgCl, reported schematically in Figure S1b:

$$\begin{aligned} FePO_{4(\alpha)} + Li^{+}{}_{(\varepsilon)} + e^{-}{}_{(\alpha)} &\rightleftarrows LiFePO_{4(\beta)} \\ AgCl_{(\beta')} + e^{-}{}_{(\alpha')} &\rightleftarrows Ag_{(\alpha')} + Cl^{-}{}_{(\varepsilon)} \end{aligned} \qquad \text{(S6)}$$

In which case the equilibrium potential does not depend on the amount of lithium extracted from the $LiFePO_4$ phase:

$$\begin{aligned} E_{+} &= E_{+,0} + \frac{RT}{F}\ln\left[a_{Li,\varepsilon}\right] \\ E_{-} &= E_{-,0} - \frac{RT}{F}\ln\left[a_{Cl,\varepsilon}\right] \end{aligned} \qquad \text{(S7)}$$

As demonstrated by the experimental results shown in Figure 4a, the total potential difference has to increase with the concentration of the LiCl salt, according to the following equation:

$$\Delta E = \Delta E_0 + \frac{RT}{F}\ln\left[a_{Li,\varepsilon}\, a_{Cl,\varepsilon}\right] \qquad \text{(S8)}$$

Using the same equations described previously, we obtained the mean activity coefficient of LiCl in water solution at different concentration, as reported in Figure S3. The value of ΔE_0 for this system is equal to 0.1784. It is interesting to observe that the activity coefficient increases at concentration above 0.5 M, which means higher concentrations of salt allows more energy to be extracted than predicted by equation (1).

2. Synthesis and characterization of the Na^+ capturing electrodes

Sodium manganese oxide, $Na_2Mn_5O_{10}$, was synthesized by soaking cotton in an aqueous solution of $NaNO_3$ (0.2 M) and $Mn(NO_3)_2$ (0.5 M). The cotton was then wrung out and heated in air in a Lindberg Moldatherm Box Furnace (Fischer Scientific) at a rate of 100 ºC h^{-1} to a final temperature of 700 ºC. This temperature was sustained for 24 hours, and then the material was allowed to cool to room temperature. The resultant powder was characterized with X-ray powder diffraction measurements using an X-ray diffractometer (XRD, Rigaku, D/MAX-IIIC X-ray diffractometer, Tokyo, Japan) with

Cu KR radiation (λ = 0.15406 nm at 45 kV and 40 mA). Representative XRD patterns are shown in Figure S4. This pattern corresponds to a mixture of phases, primarily composed of the monoclinic $Na_2Mn_5O_{10}$ phase, as reported by Parant, et al in 1971 [1], but with additional minority phases of both $Na_2Mn_3O_7$ and Mn_2O_3 [2]. We have not yet finished optimizing the synthesis conditions necessary to eliminate the presence of these minority phases, but they appear to be electrochemically inert in the conditions under which our experiments were performed. Therefore, this preliminary material is sufficient for the present work, to illustrate the feasibility of our method.

The powder was also thoroughly ground for Scanning Electron Microscopy imaging to determine the average particle size and particle morphology. SEM measurements were performed on a FEI XL30 Sirion microscope on uncoated powder samples. Images were recorded at 5 kV with a secondary electron beam. As can be seen from the images (Figure S5a-b), the conditions of our synthesis gives rise to a rod-like morphology.

Synthesis and characterization of $LiFePO_4$ will not be discussed in this work, as it is a very well know system which has been widely studied, and a wealth of information is available in literature. The $LiFePO_4$ used in this work was obtained from Alees (Advanced Lithium Electrochemistry Co., Ltd., product number LFP-NCO). It has been shown that $LiFePO_4$ is stable in neutral aqueous electrolyte, and has been tested as cathode for aqueous lithium-ion batteries[3].

3. Electrode preparation and electrochemical characterization

$Na_2Mn_5O_{10}$ and $LiFePO_4$ based electrodes were prepared by mixing the as synthesized powder of $Na_2Mn_5O_{10}$ or $LiFePO_4$ (80% wt.) with Super-P (Timcal) (9% wt.), graphite KS6 (Timcal) (3% wt.), and PVdF (8% wt.). The mixture was ball milled with a methyl methacrylate ball and vial for 1 hour. N-methyl pirrolidone (NMP) was added to the powders. The resulting slurry was stirred overnight and successively drop cast onto a carbon cloth (CC) based current collector. We used CC to avoid any

corrosion problems due to the very aggressive (chlorides) environment. After drying in oven at 100 °C for 1 hour, the electrode was ready to be tested in the electrochemical cell.

The electrochemical characterization was carried out in a three electrode cell (Figure S6). Silver gauze (chloride capturing electrode) was employed as the counter electrode (CE), $Na_2Mn_5O_{10}$ or $LiFePO_4$ based electrodes (sodium and lithium ion capturing electrodes respectively) as working electrodes (WE) and Ag|AgCl|KCl (3.5 M) as the reference electrode (RE). In the presence of the reference electrode, both working and counter electrode potentials can be monitored. The Galvani schemes are reported in Figure S1.

The geometrical electrode surface area in contact with the solution was 1 cm^2. The distance between positive and negative electrodes was 1 cm. The resistance of the electrolyte was measured by electrochemical impedance spectroscopy and was equal to 75 Ω in diluted NaCl solution (river water) and 5 Ω in concentrated NaCl solution (salt water). The high resistance measured in the diluted NaCl solution (river water) involves a high ohmic drop (about 20 mV), already outlined and discussed in the main text. The cell geometry could be improved by reducing the distance between electrodes, however, we have not yet optimized a compact cell geometry. The as-prepared $Na_2Mn_5O_{10}$ was subjected to galvanostatic cycling in order to evaluate the best operative potential range (Figure S7). It was cycled in a 0.6 M NaCl solution, using a platinum counter electrode and a Ag|AgCl|KCl (3.5 M) reference electrode. The material was originally tested up to 1.2 V (Figure S7a). It is possible to observe three small plateaus at 0.3 V, 0.6 V and 1.0 V respectively. Among these three, only the one at 0.3 V is highly reversible. Moreover, it is the best potential in terms of avoiding self discharge (at higher potentials oxygen evolution is not negligible). In Figure S7b is shown the galvanostatic cycling of the material up to 0.45 V to check its reversibility.

4. Test with collected water samples

To investigate challenges that could arise from the use of real sea water and river water (impurities, presence of other cations and anions, etc.), samples from natural water sources were tested. Salt water was obtained from Half Moon Bay, San Francisco, CA, and fresh water was collected from Donner Lake, Truckee, CA. Due to the extremely low ion content of the lake water, a small amount of sea water (2%) was premixed with the river water to obtain a reasonable conductivity of the solution. Figure S8 show the results of this test. As can be observed, the extracted energy is around 41 mJ cm^{-2} (the fresh water used contains less ions than the simulated solution, resulting in a larger gained potential), and the efficiency is 75%, essentially the same as was demonstrated in the previous laboratory test. The stability of the system in sea water was also tested. The electrodes were immersed in sea water, and allowed to equilibrate over several hours. In Fig. S9 the stability of AgCl / $Na_2Mn_5O_{10}$ in sea water is reported for a 10 hour period. During this time, the system loses 38 mV of the 186 mV it gained by the exchange of the river water with the sea water. The loss during the duration of one cycle (46 min) is around 10%. In a dynamic case, this effect would be repressed by the decrease of the potential during step 3.

REFERENCES.

1. Parant, J. P.; Olazcuaga, R.; Devalette, M.; Fouassier, C.; Hagenmuller, P. *J. Solid State Chem.* **1971,** 3, (Copyright (C) 2011 American Chemical Society (ACS). All Rights Reserved.), 1-11.
2. Chang, F. M.; Jansen, M. *Zeitschrift für anorganische und allgemeine Chemie* **1985,** 531, (12), 177-182.
3. Liu, X.-H.; Saito, T.; Doi, T.; Okada, S.; Yamaki, J.-i. *Journal of Power Sources* **2009,** 189, (Copyright (C) 2011 American Chemical Society (ACS). All Rights Reserved.), 706-710.

FIGURE CAPTIONS.

(a)	α′	β′	ε	α	
	Ag	AgCl	NaCl in H_2O	$Na_2Mn_5O_{10}$	
(b)	α′	β′	ε	β	α
	Ag	AgCl	LiCl in H_2O	$LiFePO_4$	$FePO_4$

Figure S1: Galvani representation of the electrochemical systems (a) AgCl / $Na_2Mn_5O_{10}$ and (b) AgCl / $LiFePO_4$.

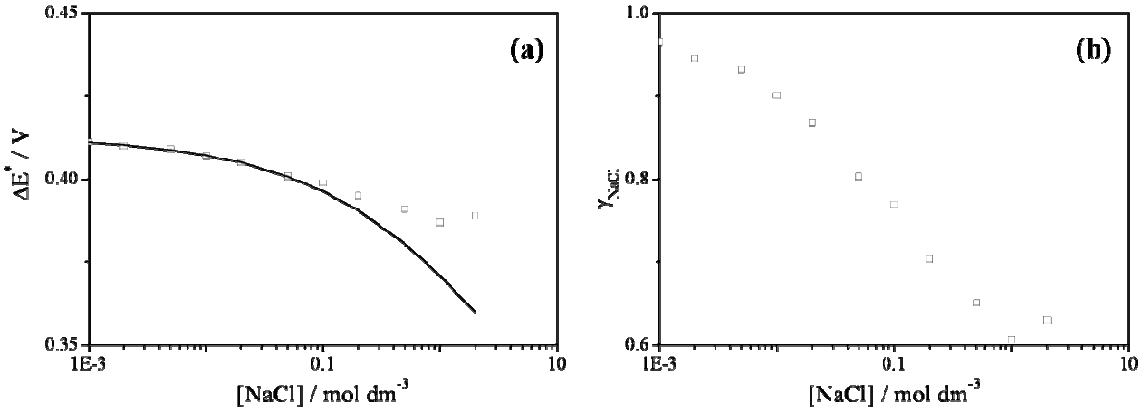

Figure S2: (a) ΔE^* (as defined in equation S3) experimentally measured (squares) and predicted by equation S4 (line) at different concentrations of NaCl, obtained at point A of figure 3c; (b) mean activity coefficient of NaCl solution at different concentrations of NaCl.

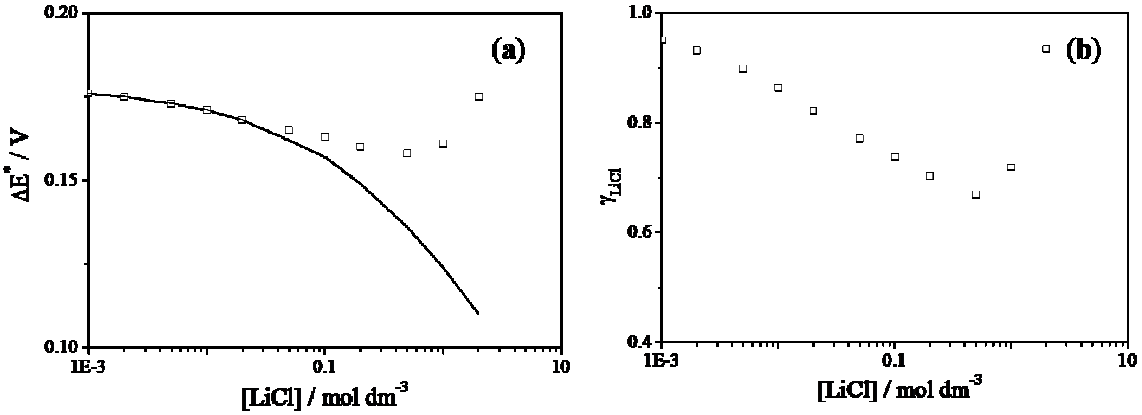

Figure S3: (a) ΔE^* (as defined in equation S3) experimentally measured (squares) and predicted by equation S4 (line) at different concentrations of LiCl; (b) mean activity coefficient of LiCl solution at different concentrations of LiCl.

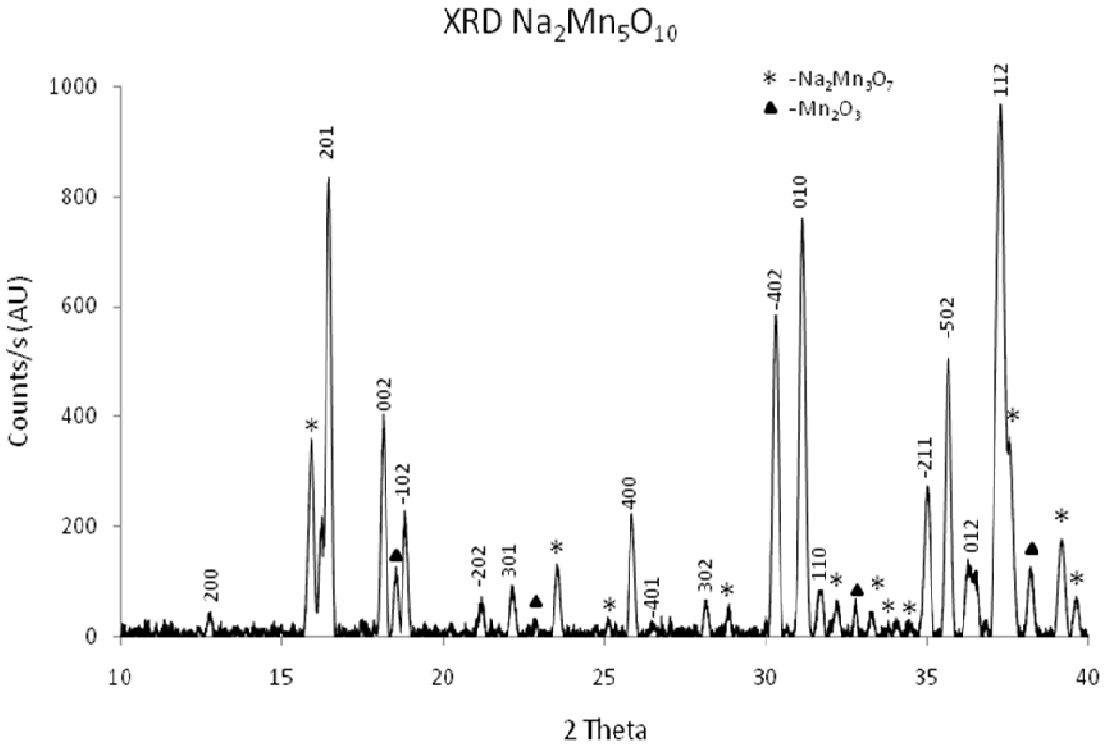

Figure S4: XRD pattern of the prepared sample, with the minority phases of $Na_2Mn_3O_7$ and Mn_2O_3 labeled.

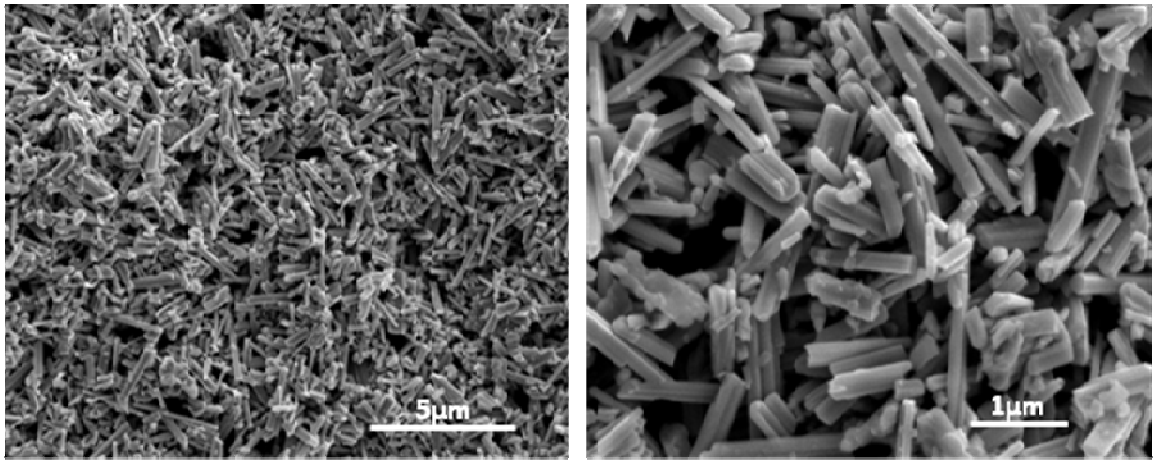

Figure S5: SEM images of the as prepared $Na_2Mn_5O_{10}$ showing (a) good uniformity of nanorod morphology throughout the sample, and (b) nanorods with an average size distribution of about 300 nm in width and 1 to 3 microns in length.

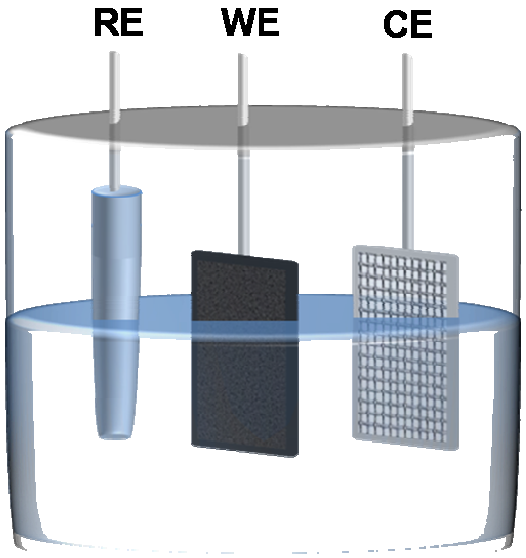

Figure S6: Schematic of cell geometry, showing the silver mesh electrode (CE), $Na_2Mn_5O_{10}$ electrode (WE), and reference electrode (RE).

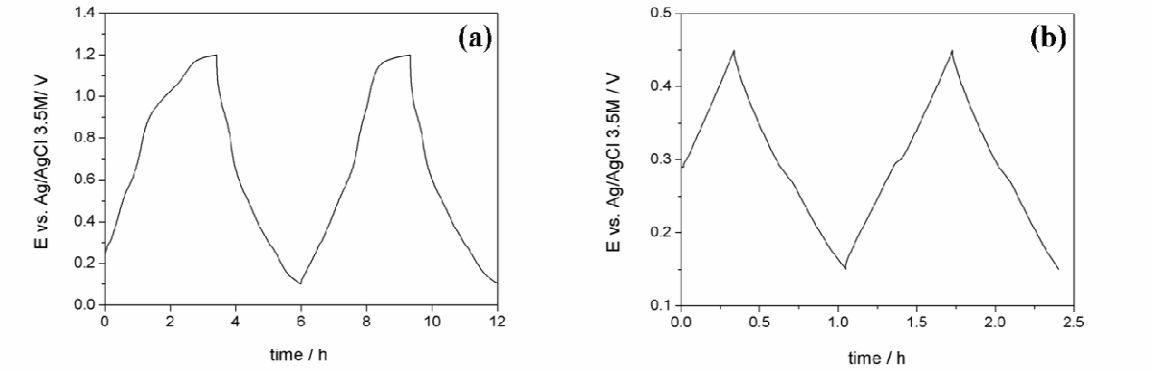

Figure S7: Galvanostatic (250 µA) cycles of $Na_2Mn_5O_{10}$ at (a) high potentials (1.2 V) and (b) low potentials (0.45 V).

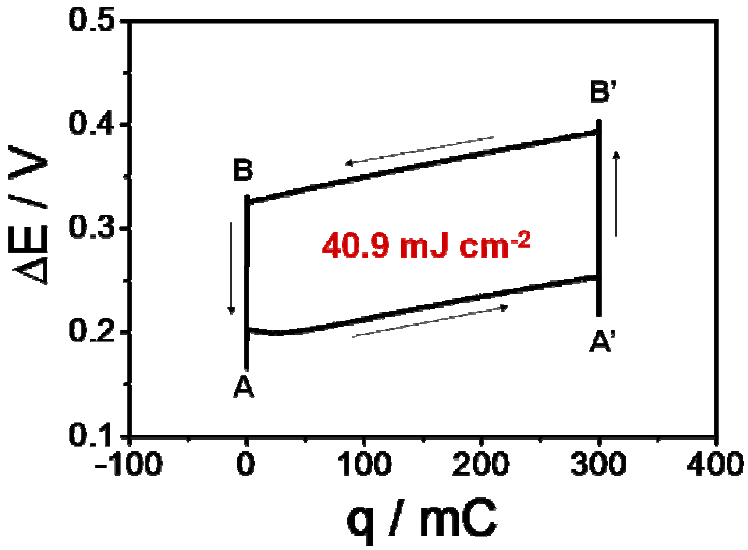

Figure S8: Real sea water/river water energy extraction cycle for the $AgCl/Na_2Mn_5O_{10}$ system in a ΔE vs. q. plot (the area is equal to the extracted energy).

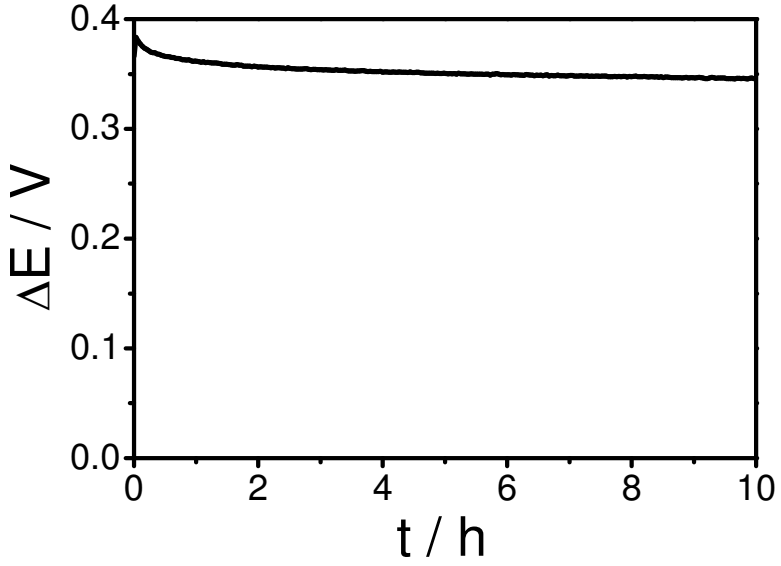

Figure S9: Stability of the AgCl / $Na_2Mn_5O_{10}$ system in an actual sea water sample.